New QP/QI Symmetric Stellarator Configurations

Donald A. SPONG and Jeffrey H. HARRIS
Oak Ridge National Laboratory, Oak Ridge, TN 37831, USA

(Received 21 December 2009 / Accepted 6 April 2010)

A unique characteristic of the quasi-poloidal/isodynamic transport optimization strategy is that it can lead to stellarators that deviate from the usual "doughnut" shape; i.e., they can have extended relatively straight cylindrical sections of plasma (connected by corner regions). This offers a number of potential design advantages, including simplified coil geometries, novel divertor approaches, low bootstrap current (less potential for ELMs and disruptions), more acceptable wall heat fluxes, and demountable blankets for reactors. The STELLOPT approach has been used to develop optimized configurations of this type for two and four field periods with aspect ratio $<R>/<a>$ in the range of 8 to 16.

Keywords: stellarator, optimization, transport, quasi-symmetry, Shafranov shift, effective ripple

DOI: 10.1585/pfr.5.S2039

1. Introduction

Modern stellarator design based on computational search methods, such as STELLOPT [1], offers a great degree of flexibility to achieve acceptable physics goals within a variety of configurational shapes. In this paper, several exploratory designs are described and analyzed that have evolved out of the QPS configuration [2]. QPS configurations have been previously shown to offer access to second stability [3, 4], high cross-field plasma flows [5] that can suppress micro-turbulence and improved stability to trapped electron instabilities [6]. The new configurations described here are also expected lead to simplified engineering and reactor technology considerations. For example, in the case of two field periods, the moderate racetrack shape (from the top view) of QPS is further elongated along its major axis, leading to sections of plasma with approximately straight cylindrical shaping. A four field period configuration has similar straight sections. This offers simplified coil geometries, improved quasi-symmetry, better compatibility with divertors, possibility for direct ion heating through magnetic beach RF absorption, and more space to accommodate the radial build from coils and structural elements.

2. Description of Equilibrium Magnetic Structure

Figure 1 shows the outer flux surface shape and filamentary coils for two ($<R>/<a> = 8$) and four ($<R>/<a> = 16$) field period devices. The flux surface shapes are based on VMEC [7] fixed boundary equilibria and the coils have been obtained from the NESCOIL [8] code (using 12 coils per period). The magnetic field strength on an outer flux surface varies by about a factor of two.

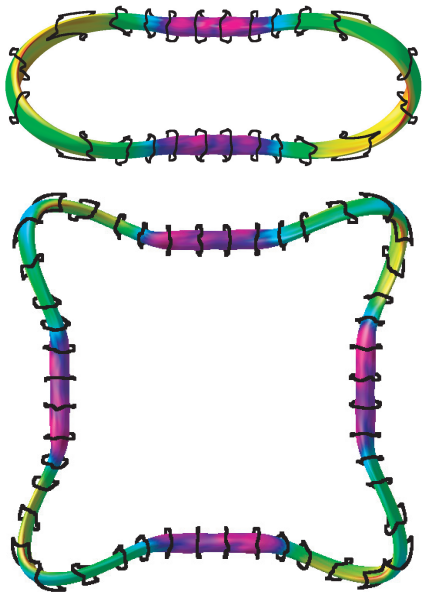

Fig. 1 Top views of two and four field configurations with outer flux surfaces and filamentary coils. The color contours indicate magnetic field strength with magenta denoting minimum values and yellow to red maximum values.

The nested fixed boundary flux surface shapes at different toroidal angles for the configurations of Fig. 1 are shown in Fig. 2 at $<\beta> = 1\%$. The rotational transform profiles for these configurations are shown in Fig. 3. Rotational transform is produced in these configurations by helical magnetic axis shaping. In transforming from the two field period to the four field period configuration, the scaling of constant ι/N_{fp} and $(<R>/<a>)/N_{fp}$ has been approximately maintained, where N_{fp} = number of field periods.

These newer devices also provide improvements in quasi-poloidal symmetry over the QPS design. This is due

author's e-mail: spongda@ornl.gov

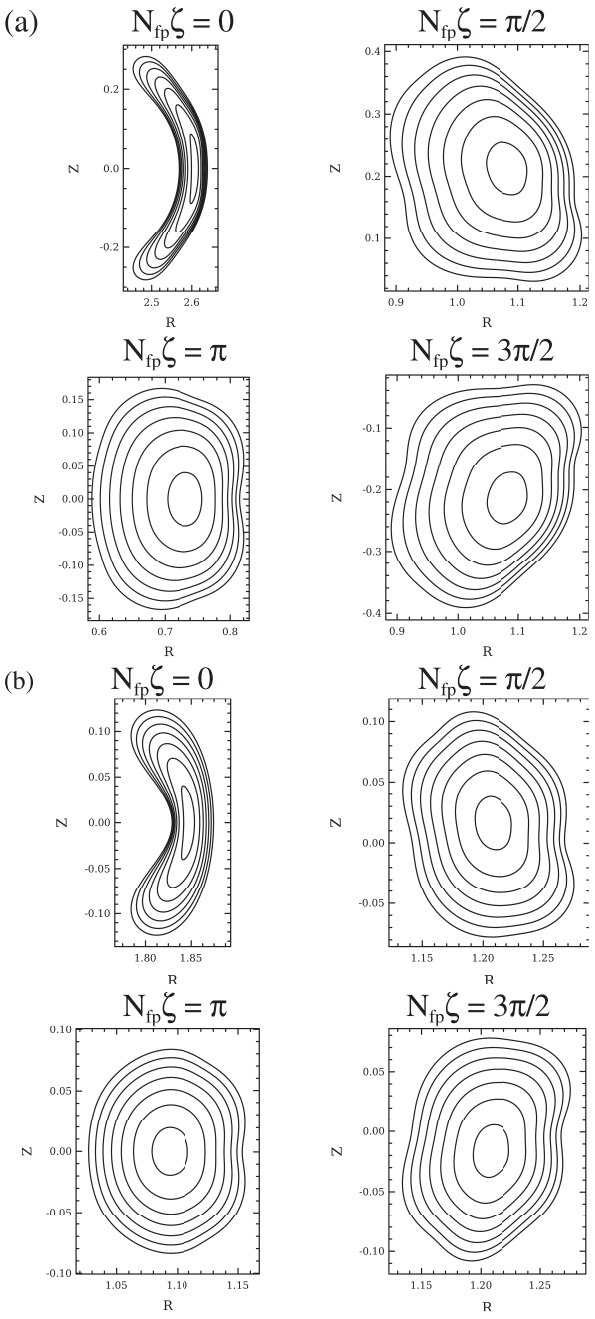

Fig. 2 Flux surface shapes at fixed toroidal angles for (a) two field periods, and (b) four field periods.

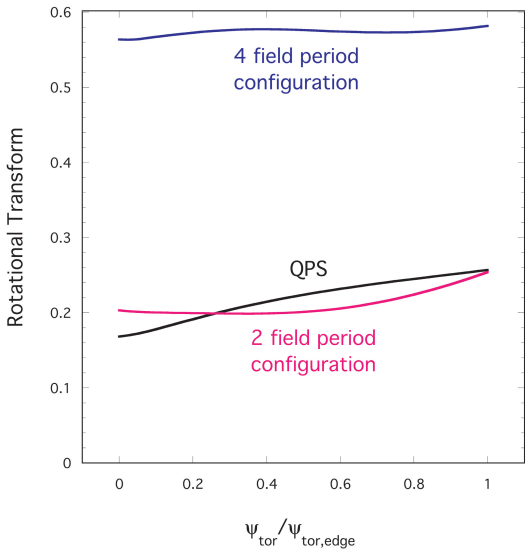

Fig. 3 Rotational transform profiles for QPS, and the new two and four field period configurations.

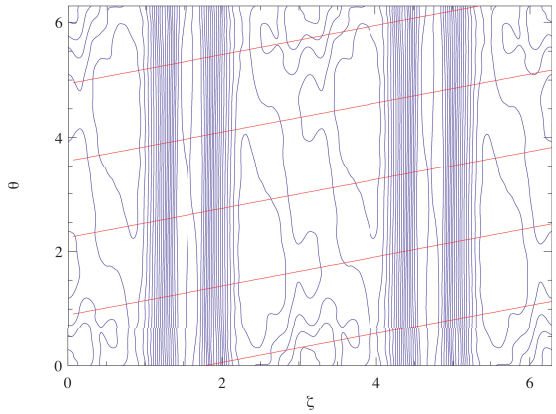

Fig. 4 Contours of $|B|$ vs. toroidal (ζ) and poloidal (θ) angles at $(\psi/\psi_{edge})^{1/2} = 0.5$, where ψ = toroidal magnetic flux, for $N_{fp} = 2$ configuration.

to the higher aspect ratios and the higher fractions of the configurational volume that are characterized by straight cylindrical geometry relative to sections with toroidally curved geometry. In the case of the two field period device, the contours of $|B|$ at $(\psi/\psi_{edge})^{1/2} = 0.5$, where ψ = toroidal magnetic flux are plotted in Boozer coordinates [9] in Fig. 4, showing a dominantly vertical structure (QP-symmetry) in the side regions (straight sections). R.M.S (root-mean square) sums over symmetric and non-symmetric $|B_{mn}|/B_0$ components for QPS and the $N_{fp} = 2$ and 4 configurations are shown in Fig. 5. As can be seen, the poloidally symmetric modes ($m = 0$), dominate over the non-symmetric modes ($m \neq 0$), and the $N_{fp} = 2$ and 4 devices have lower levels of non-symmetric components than QPS.

A final aspect of the equilibrium properties that is of interest is the variation of flux surface shape with increasing plasma <β>. In Fig. 6, a sequence of fixed boundary equilbria are shown for the $N_{fp} = 2$ configuration for <β>'s running from 0.5% to 2%. For the <β> = 2% case, the Shafranov shift has become a significant fraction of the minor radius.

A similar equilibrium sequence for the $N_{fp} = 4$ configuration is shown in Fig. 7, but for <β> running from 0.5% to 5%. In this case, very little change in the magnetic axis location can be seen. Rather a vertical compression in the surfaces is apparent as <β> is increased.

This resilience to increasing <β> is due to the lower

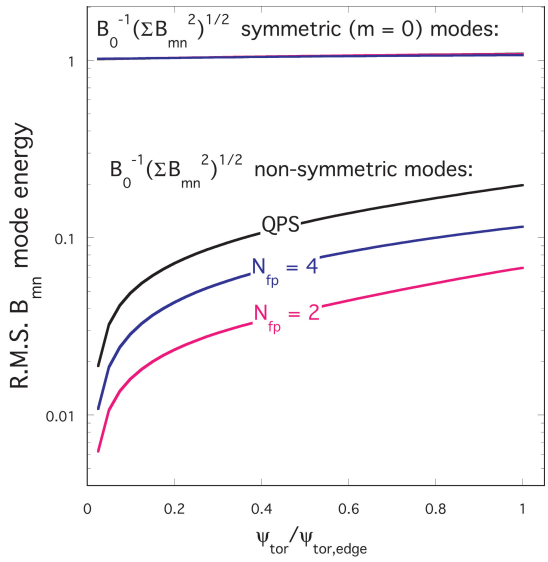

(b)

Fig. 5 R.M.S. sums of $|B_{mn}|/B_0$ modes over symmetric ($m = 0$) and non-symmetric ($m \neq 0$) modes.

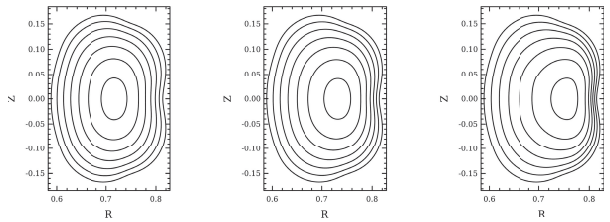

Fig. 6 Variation of magnetic surface shapes for two field periods at $N_{fp}\zeta = \pi$ cross section for $<\beta> = 0.5\%$, 1% and 2%.

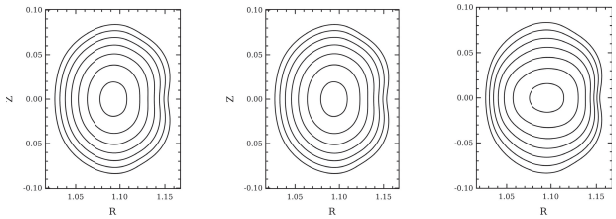

Fig. 7 Variation of magnetic surface shapes for four field periods at $N_{fp}\zeta = \pi$ cross section for $<\beta> = 0.5\%$, 1% and 5%.

level and different structure of the Pfirsch-Schlüter currents in the $N_{fp} = 4$ configuration. While the larger Shafranov shifts in the $N_{fp} = 2$ may lead to flux surface breakup at moderate values of $<\beta>$, it also has the positive effect of allowing access to second ballooning at lower $<\beta>$, as will be shown in the next section. Through continued optimization, it is expected that the larger Shafranov shifts in the $N_{fp} = 2$ device can be reduced; another possibility is control through external quadrupole vertical field coils.

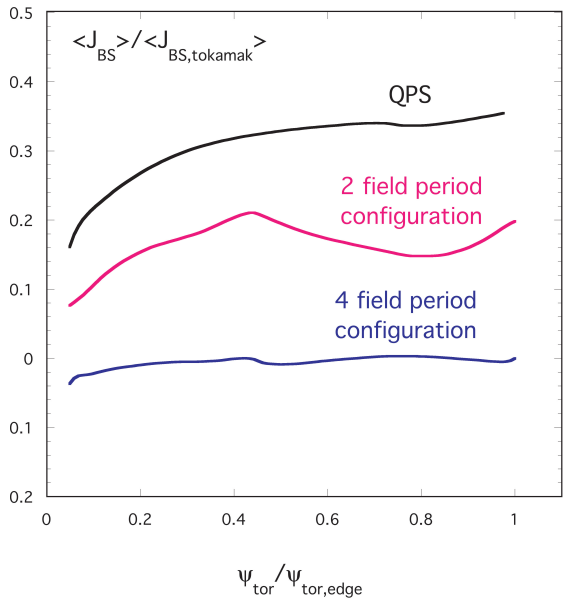

Fig. 8 Low collisionality bootstrap current profiles at $<\beta> = 1\%$ for QPS and $N_{fp} = 2$ and 4 configurations.

3. Evaluation of the Physics Properties

A number of simplified transport and stability physics characteristics of the new configurations have been evaluated. In Fig. 8, the ratio of asymptotic low collisionality bootstrap current levels to those of the equivalent tokamak are plotted vs. flux surface location. QPS was designed to be a hybrid configuration, with a small fraction of its rotational transform provided by bootstrap current and thus has the largest value of $<J_{BS}>$ in this figure.

The $N_{fp} = 4$ configuration shows a strong suppression of bootstrap current, while the $N_{fp} = 2$ configuration is in between this and QPS in its bootstrap current level. A second transport measure, and one that has been used as an optimization target for these configurations, is the effective ripple ε_{eff}, as provided by the NEO [10] code. Profiles of $\varepsilon_{eff}^{3/2}$ are plotted in Fig. 9 for several different configurations. This parameter is a geometry-dependent factor in the low-collisionality stellarator diffusion coefficient and reflects the level of ripple transport enhancement. In addition to $N_{fp} = 2$ and 4 configurations, LHD (at its normal magnetic axis location) and an $<R>/<a> = 20$ verison of the $N_{fp} = 2$ configuration are shown. As indicated, effective ripple levels in the new configurations remain higher than for QPS. This property is the subject of continuing optimization.

The results of Fig. 9 follow an opposite trend to those of Fig. 5, which indicated improved quasi-symmetry for the new $N_{fp} = 2, 4$ configurations compared to QPS. While a comprehensive understanding of this effect has not been developed, it is noted that direct measures of transport, such as $\varepsilon_{eff}^{3/2}$, involve nonlinear dependencies on the magnetic field (e.g., through the $1/B$ scaling of the drift veloc-

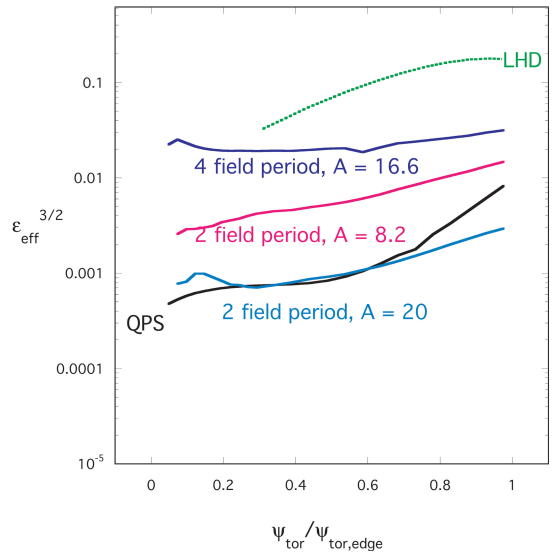

Fig. 9 Effective ripple profiles for QPS, LHD and new configurations.

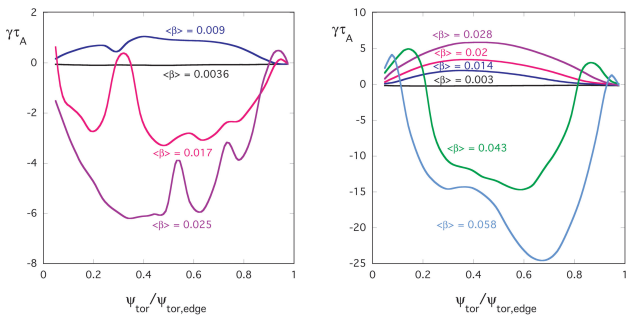

Fig. 10 Ballooning mode growth rates for $N_{fp} = 2$ (left) and $N_{fp} = 4$ (right) configurations.

ities) and thus should not be expected to have a linear correlation with improving quasi-symmetry. Also, since $\varepsilon_{eff}^{3/2}$ is related to the drift velocity, which contains derivatives of B, it may depend more strongly on certain non-symmetric modes than others, while the parameter plotted in Fig. 5 weights all non-symmetric modes equally. Future work on these configurations will also evaluate nonlocal transport mechanisms, such as energetic alpha particle losses.

With respect to stability, both Mercier and ballooning stability criteria have been targeted in the optimization, although not to the same degree as the quasi-symmetry and transport criteria. The stability boundaries for first stability ballooning are in the range of 0.6-0.7%, while Mercier boundaries are around 1%. Both configurations also have access to second ballooning stability regimes; this characteristic is shown in Fig. 10 based on results from the COBRA [11] code.

The $N_{fp} = 2$ configuration enters second stability at around $<\beta> = 1.5\%$ while the $N_{fp} = 4$ configuration accesses it around $<\beta> = 3.5\%$. The lower threshold for $N_{fp} = 2$ is caused by a deeper magnetic well induced by the more significant Shafranov shift in the $N_{fp} = 2$ device.

4. Conclusions

New two and four field period configurations are described that have been evolved from the QPS concept. These devices are currently being optimized at higher aspect ratios than QPS and have been shown to provide improved levels of quasi-symmetry. Low field period quasi-poloidal systems tend geometrically to consist of straight regions connected by curved sections. The configurations discussed here have extended the length of the straight regions. This property is expected to provide simpler modular coil geometries, greater surface-to-volume ratios, possibilities for removable blankets in reactors, options for direct ion heating through magnetic beach RF heating, improved toroidal bundle divertor design choices and less neutral beam shine-through with access for injecting on more nearly passing orbits. Optimization efforts to further improve equilibrium, transport and stability properties are underway. Also, more compact configurations with aspect ratios intermediate between QPS and these systems in this paper are being developed.

Acknowledgements

Research sponsored by the U.S. Department of Energy under Contract DE-AC05-00OR22725 with UT-Battelle, LLC. Useful discussions with Long-Poe Ku, John Canick, Raul Sanchez, Steven Hirshman, Andrew Ware and Aaron Sontag are gratefully acknowledged.

[1] S. P. Hirshman, D. A. Spong, J. C. Whitson *et al.*, Phys. Plasmas **6**, 1858 (1999).
[2] J. F. Lyon, B. E. Nelson, R. D. Benson *et al.*, Fusion Eng. Des. **82**, 575 (2007).
[3] S. R. Hudson, C. C. Hegna, R. Torasso and A. Ware, Plasma Phys. Control. Fusion **46**, 869 (2004).
[4] A. Ware, S. P. Hirshman, D. A. Spong *et al.*, Phys. Rev. Lett. **89**, 125003-1 (2002).
[5] D. A. Spong, Phys. Plasmas **12**, 056114 (2005).
[6] G. Rewoldt, L.-P. Ku and W. M. Tang, Phys. Plasmas **12**, 102512 (2005).
[7] S. P. Hirshman and J. C. Whitson, Phys. Fluids **26**, 3553 (1983).
[8] P. Merkel, Nucl. Fusion **27**, 867 (1987).
[9] A. H. Boozer, Phys. Fluids **23**, 904 (1980).
[10] V. V. Nemov, S. V. Kasilov, W. Kernbichler and M. F. Heyn, Phys. Plasmas **6**, 4622 (1999).
[11] R. Sanchez, S. P. Hirshman and A. S. Ware, J. Comput. Phys. **161**, 576 (2000).